ACS central science

Research Article

http://pubs.acs.org/journal/acscii

Hierarchical Self-Organization of AB_n Dendron-like Molecules into a Supramolecular Lattice Sequence

Xueyan Feng,[†,#] Ruimeng Zhang,[†,#] Yiwen Li,[‡,#] You-lee Hong,[⊥,∥] Dong Guo,[†] Kening Lang,[†] Kuan-Yi Wu,[†] Mingjun Huang,[†] Jialin Mao,[†] Chrys Wesdemiotis,[†] Yusuke Nishiyama,[⊥,∥] Wei Zhang,[†] Wei Zhang,[▽] Toshikazu Miyoshi,[*,†] Tao Li,[*,§] and Stephen Z. D. Cheng[*,†]

[†]Department of Polymer Science, College of Polymer Science and Polymer Engineering, The University of Akron, Akron, Ohio 44325-3909, United States

[‡]College of Polymer Science and Engineering, State Key Laboratory of Polymer Materials Engineering, Sichuan University, Chengdu 610065, China

[§]X-ray Science Division, Advanced Photon Source, Argonne National Laboratory, Argonne, Illinois, 60439, United States

[⊥]RIKEN CLST-JEOL Collaboration Center, RIKEN, Yokohama 230-0045, Japan

[∥]JEOL RESONANCE Inc., Tokyo 196-8558, Japan

[▽]South China Advanced Institute for Soft Matter Science and Technology, South China University of Technology, Guangzhou 510640, China

Supporting Information

ABSTRACT: To understand the hierarchical self-organization behaviors of soft materials as well as their dependence on molecular geometry, a series of AB_n dendron-like molecules based on polyhedral oligomeric silsesquioxane (POSS) nanoparticles were designed and synthesized. The apex of these molecules is a hydrophilic POSS cage with 14 hydroxyl groups (denoted DPOSS). At its periphery, there are different numbers (n = 1−8) of hydrophobic POSS cages with seven isobutyl groups (denoted BPOSS), connected to the apical DPOSS via flexible dendron type linker(s). By varying the BPOSS number from one to seven, a supramolecular lattice formation sequence ranging from lamella (DPOSS-BPOSS), double gyroid (space group of $Ia\bar{3}d$, DPOSS-$BPOSS_2$), hexagonal cylinder (plane group of $P6mm$, DPOSS-$BPOSS_3$), Frank−Kasper A15 (space group of $Pm\bar{3}n$, DPOSS-$BPOSS_4$, DPOSS-$BPOSS_5$, and DPOSS-$BPOSS_6$), to Frank−Kasper sigma (space group of $P4_2/mnm$, DPOSS-$BPOSS_7$) phases can be observed. The nanostructure formations in this series of AB_n dendron-like molecules are mainly directed by the molecular geometric shapes. Furthermore, within each spherical motif, the spherical core consists hydrophilic DPOSS cages with flexible linkages, while the hydrophobic BPOSS cages form the relative rigid shell, and contact with neighbors to provide decreased interfaces among the spherical motifs for constructing final polyhedral motifs in these Frank−Kasper lattices. This study provides the design principle of molecules with specific geometric shapes and functional groups to achieve anticipated structures and macroscopic properties.

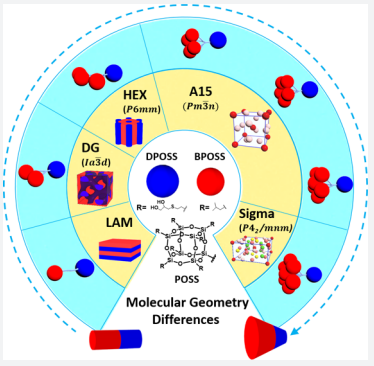

INTRODUCTION

Originally, Frank−Kasper (F−K) phases were found in metal alloys, and in principle they are sphere packing phases.[1,2] These crystal structures are topologically close packing structures that contain Frank polyhedra (icosahedra with a coordination number of 12) with one or more of the Kasper polyhedra (coordination numbers of 14, 15, or 16). More than 20 types of F−K phases have been discovered,[3] including the most common members of the A15 phase (space group of $Pm\bar{3}n$, with A_3B stoichiometry, such as Nb_3Sn), sigma phase (space group of $P4_2/mnm$, with AB stoichiometry, such as CoCr), z phase (space group of $P\bar{6}$, with A_4B_3 stoichiometry, such as Zr_4Al_3), μ phase (space group of $R\bar{3}m$, with A_6B_7 stoichiometry, such as W_6Fe_7), and many others. Among them, some of the F−K phases such as A15 and sigma phases are regarded as periodic approximants of aperiodic "quasicrystals".[4−6]

In recent years, F−K A15 and sigma phases have been found in supramolecular assemblies by many soft materials including dendrimers,[7−13] block copolymers,[14−16] liquid crystals,[17] colloidal particles,[18] giant tetrahedra[19] and giant surfactants,[20] etc. Different from those F−K phases in metal alloys where distinct sizes and electronic states of metal atoms are involved, many examples of F−K lattices in soft matters are only constructed by a single type of molecule. Those molecules first construct supramolecular spherical motifs. At this stage, size heterogeneity of the spherical motifs is supposedly introduced

Received: April 29, 2017
Published: August 7, 2017

DOI: 10.1021/acscentsci.7b00188
ACS Cent. Sci. 2017, 3, 860−867

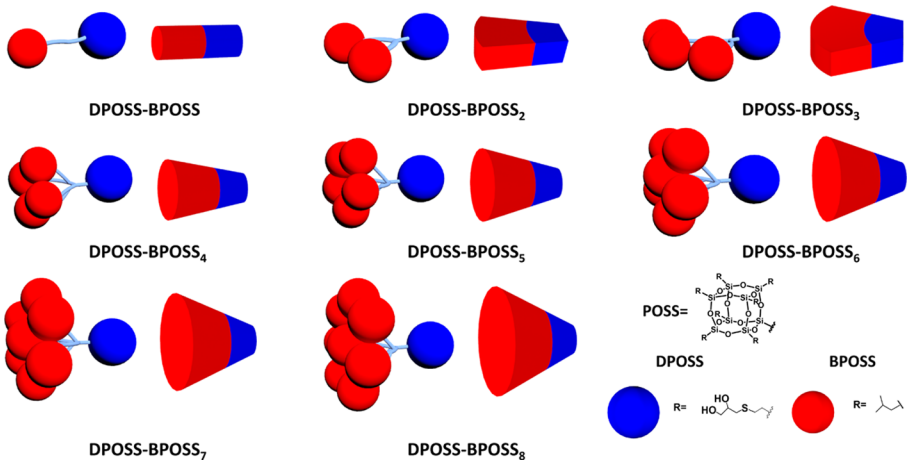

Figure 1. Molecular design of AB_n dendron-like molecules. A library of AB_n dendron-like molecules (n = 1−8) accompanied by a set of cartoons which represent the geometric shapes. With increasing the number of BPOSS cages, the geometry of the molecules changes from linear to fan-like and further to cone-like shapes.

partially due to the statistical variation of molecule numbers in one motif, as well as due to the deformable nature of these spherical motifs. Those spheres further assemble into F−K lattices, and their shape will become polyhedra in order to fill the interstitial voids of the lattices.[12,14,20,21] The formation pathway is thus a hierarchical self-assembly process. There are different ways to form the spherical motifs in general;[8,11,14,22−27] among them, one of the geometrical choices is that the molecules can have a cone-like shape, which allows the formation of core−shell type spherical motifs for further assemblies.

To achieve understanding of the formation mechanism of various nanostructures and their stability sequences in soft materials, the rational design of the molecular model system is required. Those newly designed molecules need precisely controlled molecular properties (such as topological shape, functional group, molecular weight, etc.). As discussed above, the F−K phases are sphere packing structures, but different from metal alloys, the deforming of these spherical motifs must have a great influence on the formation of F−K lattices in soft materials.[28−30] Therefore, to design molecules for F−K lattice formation, two parameters are evidently important at different length scales: the molecules must possess specific shapes to construct the spherical motifs, and these spheres must exhibit deformable features.

We have, therefore, designed and synthesized a series of molecules by chemically connecting polyhedral oligomeric silsesquioxane (POSS) nanoparticles together[31−33] (one hydrophilic POSS cage with different numbers of hydrophobic POSS cages, named AB_n dendron-like molecules, n is the number of hydrophobic POSS cages, where n = 1−8; Figure 1 shows the general molecular design, and Figure S1 shows the detailed chemical structures). As shown in Figure 1, with increasing the n number, the molecular shape changes from linear to fan-like, and further to cone-like topology. Notably, when the molecules are assembled into a sphere, the flexible linkages could provide certain deformable ability.

To connect multiple POSS nanoparticles (1−1.5 nm diameter) together, dendron-type linkers are employed. Previously, in Percec-type dendrons containing relative rigid aromatic root and soft alkyl chains at the periphery, the phase formation sequence has exhibited generation- and temperature-dependent behaviors.[7−9] In this work, we designed and synthesized a series of AB_n dendron-like molecules which start from a hydrophilic POSS cage and use similar linker(s) for constructing conjugates with an ability to tune the stoichiometry and geometry by changing the number of hydrophobic POSS cages in the periphery. It is interesting to investigate what and how nanostructures can be assembled and what the supramolecular lattice sequence would be.

RESULTS AND DISCUSSION

Figure S2 shows the detailed synthetic routes toward this set of AB_n (n = 1−8) dendron-like molecules. In brief, a monofunctionalized vinyl POSS (VPOSS) cage was linked with different numbers of hydrophobic isobutyl POSS cage(s) (BPOSS, n = 1−8) via esterification reactions and copper-catalyzed azide−alkyne cycloaddition (CuAAC) "click" chemistry. And the VPOSS cage was further functionalized with hydroxyl groups via a thiol−ene reaction to offer a hydrophilic POSS cage (DPOSS). The chemical characterizations are described in Supporting Information. In particular, the most convincing evidence for the successful synthesis is the matrix-assisted laser desorption/ionization time-of-flight (MALDI-TOF) mass spectra for this set of VPOSS-$BPOSS_n$ (n = 1−8) molecules. As shown in Figure S3, there is only one strong peak for each molecule, and the observed molecular mass matches well with the calculated molecular mass. The results indicate the precisely defined and uniform molecular mass of these samples. The samples were also fully characterized by ^{1}H-nuclear magnetic resonance (NMR) and ^{13}C NMR to further confirm their structural precision and high purity (Figures S4−S7). Linkages between the hydrophilic and hydrophobic POSS cages are specifically designed to be flexible in this set of molecules.

To identify the self-assembled lattices, both small-angle X-ray scattering (SAXS) and bright field transmission electron microscopy (TEM) experiments were performed. The SAXS experiments were carried out in situ on a synchrotron X-ray beamline at elevated temperatures (preventing the crystallization of BPOSS which will disturb the formation of curved motifs in complex structures;[19] the corresponding differential scanning calorimetry (DSC) data are in Figure S8). The samples were then quenched into liquid nitrogen and microtomed for the TEM observations (detailed sample preparation and experimental setup are in Supporting

DOI: 10.1021/acscentsci.7b00188
ACS Cent. Sci. 2017, 3, 860−867

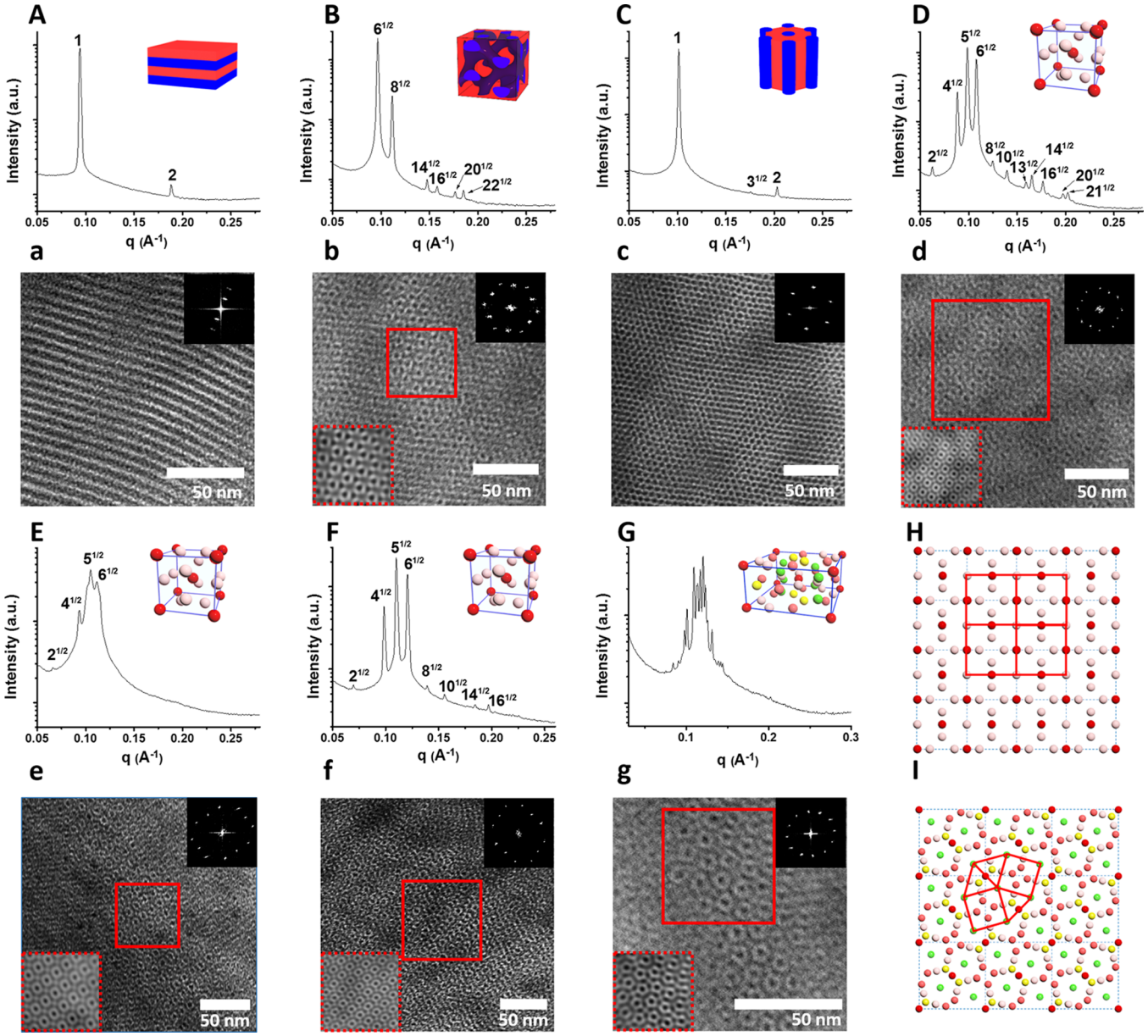

Figure 2. Self-assembled supramolecular structures of AB_n dendron-like molecules. DPOSS−BPOSS shows the LAM structure in the SAXS pattern (A) and bright field TEM images (a); DPOSS-$BPOSS_2$ shows DG structure in B (SAXS) and b (TEM); DPOSS-$BPOSS_3$ shows HEX structure in C (SAXS) and c (TEM); DPOSS−$BPOSS_4$, DPOSS−$BPOSS_5$, and DPOSS−$BPOSS_6$ all exhibit F−K A15 structure in D, E, and F (SAXS) and d, e, and f (TEM), respectively; DPOSS−$BPOSS_7$ shows F−K sigma structure in G (SAXS) and g (TEM). In the SAXS patterns, cartoons corresponding to different lattices are inserted: colors in A, B, C indicate the hydrophilic domain (blue) and hydrophobic domain (red); colors in D, E, F, G indicate lattice sites with different local coordination environments. In TEM images, they are along the [111] direction of the DG in b, the [001] direction of the HEX in c, the [001] direction of the A15 in d, e, and f, and the [001] direction of the sigma in g. The upper right insets of the TEM images are corresponding FFT patterns and the bottom left insets in b, d, e, f and g are the local TEM image after Fourier filtering. H is 2D-projected cartoon view of the A15 lattice along the [001] direction, a 4^4 tiling element is highlighted with red line; I is 2D-projected cartoon view of the Sigma lattice along the [001] direction, a $3^2.4.3.4$ tiling element is highlighted with red line.

Information). Figure 2 shows a set of SAXS patterns in reciprocal space and the corresponding bright field TEM images in real space for this series of samples. The SAXS patterns are shown in the form of intensity (I) versus scattering vector magnitude $|\vec{q}| = q = 4\pi\lambda^{-1} \sin(\theta/2)$, where θ is the scattering angle and λ is the radiation wavelength. The TEM results show the typical structure images along certain directions corresponding to each nanostructure.

Starting with the DPOSS−BPOSS sample with one DPOSS and one BPOSS, the diffraction peaks with relative positions $q/q^* = 1, 2$ (where q^* is the location of primary peak) in the SAXS pattern (Figure 2A), as well as the TEM image of microtomed thin film sample with its fast Fourier transform (FFT) pattern (Figure 2a) suggest a lamellar (LAM) structure. The long period of this LAM structure is 6.7 nm based on the SAXS result. It can be deduced that each long period of the LAM structure contains two layers of DPOSS−BPOSS with amphiphilic interactions (detailed calculations are in Supporting Information). This result is consistent with other similar AB-type POSS systems as previously reported.[34]

DOI: 10.1021/acscentsci.7b00188
ACS Cent. Sci. 2017, 3, 860−867

Table 1. Summary of Supramolecular Structures of AB_n Dendron-like Molecules

DPOSS−$BPOSS_n$	lattice	lattice dimension (nm)[a]	motif dimension (nm)[b]	M[c]	θ[d] (deg)	ρ_s[e] (nm^{-2})
DPOSS−BPOSS	LAM	6.69				0.95
DPOSS−$BPOSS_2$	DG	15.97				
DPOSS−$BPOSS_3$	HEX	6.21	6.21	5		0.70
DPOSS−$BPOSS_4$	A15	14.27^3	8.86	44	16.4	0.72
DPOSS−$BPOSS_5$	A15	13.44^3	8.34	32	22.5	0.72
DPOSS−$BPOSS_6$	A15	12.78^3	7.93	24	30.0	0.72
DPOSS−$BPOSS_7$	sigma	$23.62^2 \times 12.49$	7.63	18	40.0	0.70
DPOSS−$BPOSS_8$	disorder					

[a]Values are the corresponding lamellar lattice parameter, hexagonal columnar lattice parameter in HEX lattice, cubic lattice parameters in DG, A15, tetragonal lattice parameters perpendicular to and along the 4_2 screw axis in sigma phase; [b]Values are the columnar diameter in HEX lattices, spherical diameter in A15 and sigma lattice. [c]Values are the average number of AB_n dendron-like molecules within 1 nm-thick cross-section of the cylinders in hexagonal columnar lattices, and the calculated average numbers of AB_n dendron-like molecules per supramolecular sphere in A15 and sigma lattice. [d]Values are the solid angle of the cone-like shape AB_n dendron-like molecules in A15 and sigma lattice.[35,36] [e]Values are the averaged surface packing density of BPOSS cages in different structures.

When BPOSS number becomes two, DPOSS−$BPOSS_2$, the volume fraction of hydrophobic BPOSS cages increases (V_f^{BPOSS} = 48.3%, Table S1), and the sample exhibits a double gyroid (DG) structure (space group of $Ia\bar{3}d$, with parameter a = 15.97 nm) at elevated temperature. The ratios of q values where the X-ray pattern displays peaks are $\sqrt{6} : \sqrt{8} : \sqrt{14} : \sqrt{16} : \sqrt{20} : \sqrt{22}$ (Figure 2B, in situ SAXS patterns at different temperatures are in Figure S9a), which agrees with the assignment of a DG lattice. The DG structure are also confirmed by TEM image as shown in Figure 2b. A typical "wagon wheel" image and the corresponding FFT pattern from the [111] direction of DG lattice can be observed. An enlarged image of a local TEM image after Fourier filtering is also shown in the bottom left insert of Figure 2b.

With increasing the BPOSS number to three (DPOSS−$BPOSS_3$), the SAXS pattern shows diffraction peaks of (q/q^*) = $1 : \sqrt{3} : 2$ at elevated temperature (Figure 2C, in situ SAXS patterns at different temperatures are in Figure S9b). These peaks are consistent with a hexagonal cylinder (HEX) lattice (with plane group of $P6mm$). This is also confirmed by bright field TEM image with an FFT pattern showing 6-fold symmetry (Figure 2c). Note that this AB_3 molecule now exhibits a fan-like shape.

Further increasing the BPOSS number to four, DPOSS−$BPOSS_4$, the SAXS pattern displays diffraction peaks at places where relative q/q^* ratios are $\sqrt{2} : \sqrt{4} : \sqrt{5} : \sqrt{6} : \sqrt{8} : \sqrt{10} : \sqrt{13} : \sqrt{14} : \sqrt{16} : \sqrt{20} : \sqrt{21}$, again at the elevated temperature (Figure 2D, in situ SAXS patterns at different temperatures are in Figure S9c). On the basis of previous studies,[11,19] this pattern can be assigned as a F−K A15 lattice (space group of $Pm\bar{3}n$) with a cubic unit cell (a = 14.27 nm). The lattice assignment is further validated by the TEM image of the microtomed sample with its corresponding FFT pattern and a local TEM image after Fourier filtering (Figure 2d). The TEM image after Fourier filtering treatment (in the bottom left insert of Figure 2d) shows a clear two-dimensional (2D) image that can be tiled using 4^4 tiling elements which contain four squares, in accordance with the 2D A15 cartoon pattern along the [001] direction (Figure 2H). The FFT pattern (in the upper right insertion of Figure 2d) shows a typical pattern for A15 lattice along the [001] direction. Compared with DPOSS−$BPOSS_3$, the volume fraction of hydrophobic part in this sample is larger (V_f^{BPOSS} = 61.4%, Table S1). The molecular geometry starts adopting a cone-like shape, and the molecules could self-assemble into core−shell spherical motifs during the initial stage of the process. Though the size of spheres in F−K A15 lattice possesses a minor difference, the size ratio of different spheres is close to 1.[19] We could thus calculate the average parameters to characterize each sphere. Here the average diameter of each sphere is estimated to be 8.86 nm. The average number of molecules in each spherical motif is about 44; namely, there are 176 BPOSS cages in one spherical motif on average. The solid angle of each molecule is calculated as 16.4° (Table 1, detailed calculations are in Supporting Information).

For DPOSS−$BPOSS_5$ and DPOSS−$BPOSS_6$, they remain in forming A15 lattices (SAXS patterns in Figure 2E,F and TEM results in Figure 2e,f). On the basis of their lattice dimensions (Table 1) and measured densities (Table S1), the average number of molecules in each spherical motif as well as the solid angle of each molecule can also be calculated (Table 1, detailed calculations are in Supporting Information). Interestingly, in A15 lattices, with increasing the number of BPOSS in one molecule (DPOSS−$BPOSS_4$ to DPOSS−$BPOSS_5$ and further to DPOSS−$BPOSS_6$), the calculated average number of molecules in each spherical motif decreases (44, 32, and 24, respectively, Table 1) as well as the total average number of BPOSS cages in each spherical motif (176, 160, and 144, correspondingly). Meanwhile, the solid angle for each cone-like molecule increases (16.4°, 22.5°, and 30.0°, Table 1). This is expected since fewer cone-shaped molecules are needed to construct a spherical motif as the solid angle increases.

If we continue to add one more BPOSS cage to the system (DPOSS−$BPOSS_7$), a SAXS pattern with more than a dozen diffraction peaks appears at elevated temperature (Figure 2G, in situ temperature-dependent SAXS results are in Figure S9f). The diffractions can be clearly indexed based on a F−K sigma phase (space group of $P4_2/mnm$) (Figure S10 and Table S2) according to previous studies.[12,14,20] Figure 2I shows a 2D cartoon feature view of the sigma phase along the [001] direction. The basic tiling elements are $3^2.4.3.4$, which contain two triangles, a square, a triangle, and a square. The TEM image (Figure 2g) confirms the formation of sigma phase with the typical $3^2.4.3.4$ tiling element as shown in Figure 2I, and the FFT image (the inset of Figure 2g) shows a typical pattern for the sigma phase along the [001] direction. We could also use the average parameters to characterize each sphere as in the case of the F−K A15 phase. The calculated average number of molecules in each spherical motif within this F−K sigma lattice is further decreased to about 18 with 126 BPOSS cages, and the

DOI: 10.1021/acscentsci.7b00188
ACS Cent. Sci. 2017, 3, 860−867

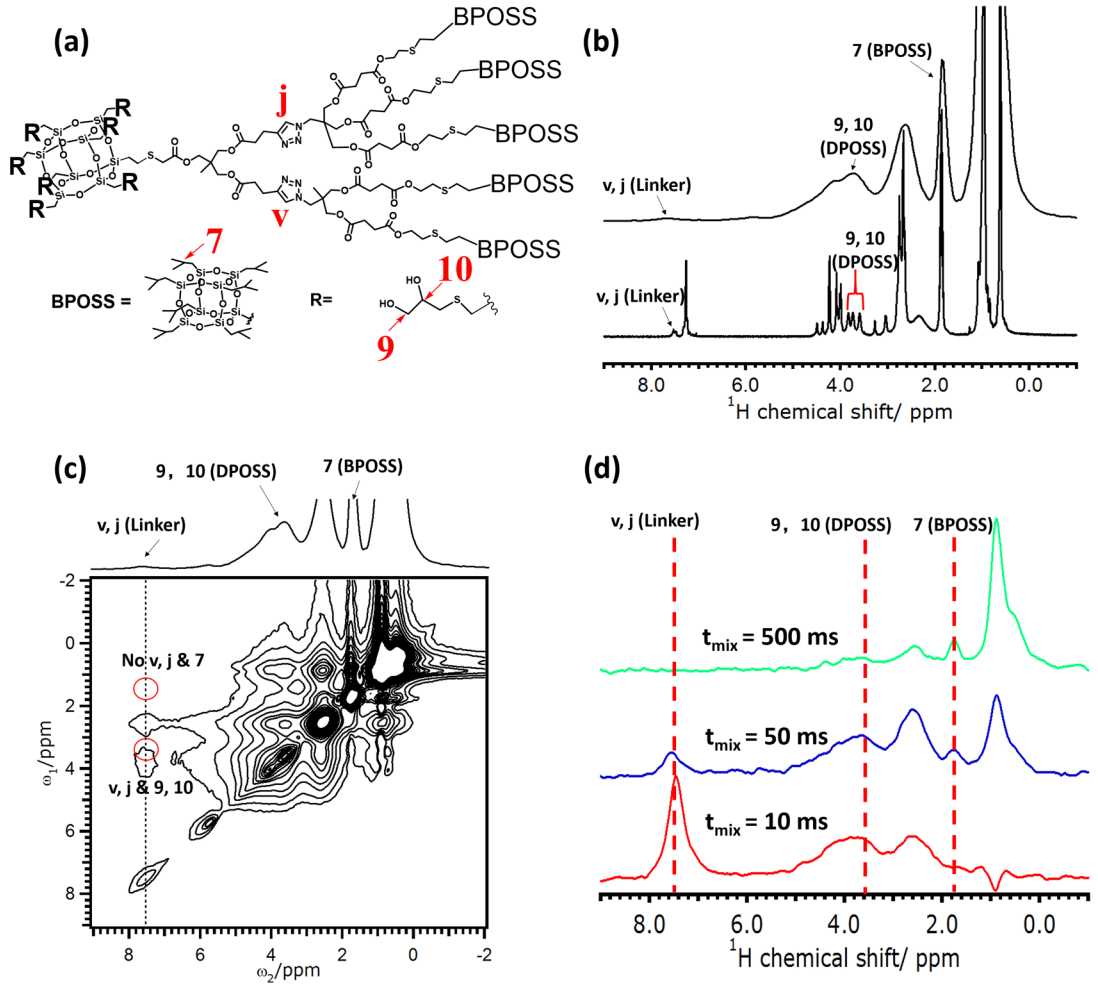

Figure 3. Molecular level spatial information on DPOSS-BPOSS$_5$ molecule in the F−K A15 phase. (a) Chemical structure of DPOSS−BPOSS$_5$, (b) ^{1}H solid-state MAS NMR spectra (up) and ^{1}H solution state NMR spectra (bottom), (c) 2D NOESY at the mixing time (t_{mix}) of 10 ms. (d) Slice data at δ = 7.5 ppm (protons v and j) extracted from the 2D NOESY spectra with different mixing times.

solid angle for each molecule becomes 40.0° (Table 1, detailed calculations are in Supporting Information). It is important to note that the volume fraction of hydrophobic part in this sample is only slightly changed (0.8%) compared with that of DPOSS−BPOSS$_6$ (Table S1).

As for DPOSS−BPOSS$_8$, the sample becomes disordered, disregarding extensive thermal and solvent annealing work (SAXS results are in Figure S11). Notably, the volume fraction of hydrophobic BPOSS part now reaches 70.3%, that is only 1.6% different from that of DPOSS−BPOSS$_7$ (Table S1). These slight changes in hydrophobic part volume fraction (between DPOSS−BPOSS$_6$ and DPOSS−BPOSS$_7$ as well as between DPOSS−BPOSS$_7$ and DPOSS−BPOSS$_8$) may trigger substantial variations of the interactions, affect the size and formation of spherical motifs, and alter the assembly pathways to form different phase structures.

In these sphere packing F−K structures, one remaining issue is that how do the cone-shaped molecules pack into a core−shell spherical motif (i.e., the spatial relationship between DPOSS, BPOSS and linkages). In every case where the F−K phases are formed, one spherical motif contains 20−50 molecules, namely, 20−50 DPOSS cages (rigid nanocages with 1.5 nm diameter) are packed together via the driving force of collective hydrogen bonding formation. Nevertheless, if one considers that DPOSSs are packed regularly in a certain order and the linkages are completely separated from the hydrophilic DPOSS cages, the only packing possibility for such a large number of DPOSS cages is to form a hollowed structure. However, this is certainly not the correct structure, since the material's bulk density had to be much lower than the currently measured values (Table S1, the experimentally measured materials' densities are in the vicinity of 1.2 g/cm^3 versus 1.43 g/cm^3 and 1.13 g/cm^3 for DPOSS and BPOSS alone, respectively). We thus employed the solid-state nuclear magnetic resonance (NMR) spectroscopy to investigate the spatial proximity of different parts (DPOSS cages, linkages, and BPOSS cages) in this series of samples. Figure 3 shows the NMR results for DPOSS−BPOSS$_5$ with F−K A15 lattice as an example. Figure 3b shows the solution ^{1}H NMR and ^{1}H solid-state magic-angle spinning (MAS) NMR spectrum of DPOSS−BPOSS$_5$. Both spectra possess almost identical chemical shifts (fully assignment of chemical shift in Figure S6e). Herein, we chose protons v and j (δ = 7.5 ppm) which are on the triazole group (in the middle of linkage) as the probe of the linkage part, protons 9 and 10 (δ = 3.6 ppm) as the probe of the DPOSS cage part and proton 7 (δ = 1.8 ppm) as the probe of the BPOSS cage part to study the spatial connectivity among DPOSS, BPOSS, and linkages (Figure 3a).

Two-dimensional (2D) nuclear Overhauser effect spectroscopy (NOESY) experiments using conventional three pulses

DOI: 10.1021/acscentsci.7b00188
ACS Cent. Sci. 2017, 3, 860−867

were carried out for the measurement of spin exchanges among different protons.[37] If two protons are spatially close to each other at several angstroms, a spin exchange signal could be observed during a short mixing time. In principle, a longer internuclear distance requires longer mixing time which induces spin exchange. Figure 3c shows the 2D NOESY spectrum at a mixing time of 10 ms, and Figure 3d shows the slice data along protons v and j (δ = 7.5 ppm, linker part) at different mixing times. At a mixing time of 10 ms, cross peaks were observed between the DPOSS part (protons 9 and 10) and the linkage part (protons v and j), and the intensities reach the quasi-equilibrium state at t_{mix} = 50 ms (Figure 3d), indicating that the DPOSS cages and linkages are at least partially mixed. The spin exchange signals between BPOSS cages (proton 7) and linkages (protons v and j) at 10 ms are absent, while the signals start to appear at t_{mix} = 50 ms. And with further increasing t_{mix} up to 500 ms, intensities of DPOSS and linker protons largely decrease concomitant with increasing BPOSS intensities. These indicate the nanophase separation between BPOSSs and linkages. A similar spatial relationship between DPOSS, BPOSS, and linkage were also observed in other kinds of AB_n dendron-like molecules (Figures S12 and S13). All these NMR results reveal that DPOSS cages are largely mixed with the linkages in the spherical core, and BPOSS cages are nanophase separated from the core to form the shell of the spherical motifs. There should also be a connecting interface of the linkages between the core and the shell. And the soft linkages in these molecules can serve as the deformable zone.

For this set of AB_n dendron-like molecules, by changing the number of BPOSS cages, the molecular geometry of samples can be systematically changed in a stepwise and uniform way, from a linear shape to a fan-like shape and further to a cone-like shape. Similar to a Percec-type dendron system,[8,9,13,38] the geometrical difference is the key issue for these molecules to form lamella, cylinder, or sphere packing structures. However, in the sphere packing region, a better theoretical understanding of the origin of the unconventional sphere packing phases (such as F−K A15 phase and sigma phase) by cone-shaped molecules is still keenly needed. This set of molecules reported here may provide some new insights.

For all four samples that exhibit sphere packing lattices, the BPOSS shell is incompressible (i.e., the thickness of BPOSS shell is fixed) due to the rigid nature of the BPOSS cage. This is quite different from previously reported samples which have soft shells.[7,9,14,15,20]

In these AB_n dendron-like molecules, there are mainly two parameters with significant influence on the phase formations: (1) the interfacial tension between the hydrophilic domain and hydrophobic domain (Υ_1), which is proportional to both the interaction parameter (χ) and the overall interfacial area between the hydrophilic core and the hydrophobic shell (S_1);[20] (2) the bulk free energy of spherical motif packing structures (F_{bulk}), which is inversely proportional to the packing efficiency (or the overall interfacial area between spherical motifs, S_2).[28,30] On the basis of the assumption of the constant value of χ, the formed spherical motif with smaller S_1 leads to a smaller Υ_1; while the spherical phase with a reduced S_2 causes a higher F_{bulk}. Since the BPOSS shell is relatively rigid as discussed above, the S_1 would be proportional to the S_2. Therefore, a smaller S_1 (i.e., a smaller S_2) would lead to a smaller Υ_1 and a higher F_{bulk}. The structure stability is thus determined by a balance between the Υ_1 and the F_{bulk}, where both parameters (Υ_1 and F_{bulk}) are associated with S_1 (or S_2). It is known that F−K A15 and sigma phases possess smaller overall interfacial areas among neighboring motifs compared with other spherical structures (such as body-centered cubic structure),[14,30] the formation of the F−K A15 and sigma phases in these AB_n dendron-like molecules would select a kinetic pathway to balance a lower interfacial tension (Υ_1) at the penalty of a relatively higher bulk free energy (F_{bulk}) for reaching a thermodynamic minimum in the overall free energy.

CONCLUSIONS

Combining the atomic spatial relationship from solid-state NMR and the lattice structure information based on SAXS and TEM results, a clear structure formation picture could be achieved. Linkages are largely mixed with DPOSS cages as the hydrophilic domain and the BPOSS part is nanophase separated from the hydrophilic domain as the hydrophobic domain. Driven by the phase separation, different supramolecular structures could be formed with the change of molecular geometry. By increasing the number of hydrophobic BPOSS cages in this set of molecules, the geometry shape of the whole molecule changes from a linear shape to a fan-like shape, and further to a cone-like shape with different solid angles. A LAM → DG → HEX → A15→ sigma → disorder phase sequence could be observed. In the sphere packing region, the geometric cone-shape of the molecules enables the formation of the first assembly into supramolecular spherical motifs, and the flexible linkages which are mainly mixed in the hydrophilic domain provide a zone for deformation in order to further assemble into F−K lattices. In addition, the tiny change of volume fraction for hydrophobic BPOSS cages between DPOSS−$BPOSS_6$ and DPOSS−$BPOSS_7$ (as well as between DPOSS−$BPOSS_7$ and DPOSS−$BPOSS_8$) with distinct structure behaviors also suggests that geometry plays the key role in these structure formations. This set of samples thus provides a model system to understand the structural evolution pathways and relationships among different phases, especially the complex F−K A15 and sigma phases. They may also offer the opportunities to design and synthesize functional molecules with certain microscopic assembly structures, and further introduce macroscopic properties to the materials.

ASSOCIATED CONTENT

Supporting Information

The Supporting Information is available free of charge on the ACS Publications website at DOI: 10.1021/acscentsci.7b00188.

Synthetic procedures, characterization methods, detailed calculation and data (PDF)

AUTHOR INFORMATION

Corresponding Authors

*E-mail: scheng@uakron.edu (S.Z.D.C.).
*E-mail: taoli@aps.anl.gov (T.L.).
*E-mail: miyoshi@uakron.edu (T.M.).

ORCID

Yiwen Li: 0000-0002-6874-0350
Toshikazu Miyoshi: 0000-0001-8344-9687
Stephen Z. D. Cheng: 0000-0003-1448-0546

Author Contributions

#X.F., R.Z., and Y.L. contributed equally to this work.

Notes

The authors declare no competing financial interest.

DOI: 10.1021/acscentsci.7b00188
ACS Cent. Sci. 2017, 3, 860−867

■ ACKNOWLEDGMENTS

This work was supported by NSF DMR-1408872 (to S.Z.D.C) and NSFC (51603133 to Y.L.), Grant-in Aid for JSPS Research Fellow 16F16047 (to Y.H.). Use of the Advanced Photon Source at Argonne National Laboratory was supported by the U.S. Department of Energy (DOE), Office of Science, and Office of Basic Energy Sciences

■ REFERENCES

(1) Frank, F. C.; Kasper, J. S. Complex alloy structures regarded as sphere packings. I. Definitions and basic principles. *Acta Crystallogr.* **1958**, *11*, 184−190.
(2) Frank, F. C.; Kasper, J. S. Complex alloy structures regarded as sphere packings. II. Analysis and classification of representative structures. *Acta Crystallogr.* **1959**, *12*, 483−499.
(3) Dutour Sikiric, M.; Delgado-Friedrichs, O.; Deza, M. Space fullerenes: a computer search for new Frank-Kasper structures. *Acta Crystallogr., Sect. A: Found. Crystallogr.* **2010**, *66*, 602−615.
(4) Gillard, T. M.; Lee, S.; Bates, F. S. Dodecagonal quasicrystalline order in a diblock copolymer melt. *Proc. Natl. Acad. Sci. U. S. A.* **2016**, *113*, 5167−5172.
(5) Zeng, X. B.; Ungar, G.; Liu, Y. S.; Percec, V.; Dulcey, A.; Hobbs, J. K. Supramolecular dendritic liquid quasicrystals. *Nature* **2004**, *428*, 157−160.
(6) Zhang, J.; Bates, F. S. Dodecagonal quasicrystalline morphology in a poly(styrene-b-isoprene-b-styrene-b-ethylene oxide) tetrablock terpolymer. *J. Am. Chem. Soc.* **2012**, *134*, 7636−7639.
(7) Sun, H.-J.; Zhang, S. D.; Percec, V. From structure to function via complex supramolecular dendrimer systems. *Chem. Soc. Rev.* **2015**, *44*, 3900−3923.
(8) Rosen, B. M.; Wilson, C. J.; Wilson, D. A.; Peterca, M.; Imam, M. R.; Percec, V. Dendron-mediated self-assembly, disassembly, and self-organization of complex systems. *Chem. Rev.* **2009**, *109*, 6275−6540.
(9) Ungar, G.; Zeng, X. B. Frank-Kasper, quasicrystalline and related phases in liquid crystals. *Soft Matter* **2005**, *1*, 95−106.
(10) Hudson, S. D.; Jung, H. T.; Percec, V.; Cho, W. D.; Johansson, G.; Ungar, G.; Balagurusamy, V. S. K. Direct visualization of individual cylindrical and spherical supramolecular dendrimers. *Science* **1997**, *278*, 449−452.
(11) Balagurusamy, V. S. K.; Ungar, G.; Percec, V.; Johansson, G. Rational design of the first spherical supramolecular dendrimers self-organized in a novel thermotropic cubic liquid-crystalline phase and the determination of their shape by X-ray analysis. *J. Am. Chem. Soc.* **1997**, *119*, 1539−1555.
(12) Ungar, G.; Liu, Y. S.; Zeng, X. B.; Percec, V.; Cho, W. D. Giant supramolecular liquid crystal lattice. *Science* **2003**, *299*, 1208−1211.
(13) Rosen, B. M.; Wilson, D. A.; Wilson, C. J.; Peterca, M.; Won, B. C.; Huang, C. H.; Lipski, L. R.; Zeng, X. B.; Ungar, G.; Heiney, P. A.; Percec, V. Predicting the structure of supramolecular dendrimers via the analysis of libraries of AB_3 and constitutional isomeric AB_2 biphenylpropyl ether self-assembling dendrons. *J. Am. Chem. Soc.* **2009**, *131*, 17500−17521.
(14) Lee, S.; Bluemle, M. J.; Bates, F. S. Discovery of a Frank-Kasper Sigma phase in sphere-forming block copolymer melts. *Science* **2010**, *330*, 349−353.
(15) Lee, S.; Leighton, C.; Bates, F. S. Sphericity and symmetry breaking in the formation of Frank-Kasper phases from one component materials. *Proc. Natl. Acad. Sci. U. S. A.* **2014**, *111*, 17723−17731.
(16) Chanpuriya, S.; Kim, K.; Zhang, J.; Lee, S.; Arora, A.; Dorfman, K. D.; Delaney, K. T.; Fredrickson, G. H.; Bates, F. S. Cornucopia of nanoscale ordered phases in sphere-forming tetrablock terpolymers. *ACS Nano* **2016**, *10*, 4961−4972.
(17) Cheng, X. H.; Diele, S.; Tschierske, C. Molecular design of liquid-crystalline block molecules: Semifluorinated pentaerythritol tetrabenzoates exhibiting lamellar, columnar, and cubic mesophases. *Angew. Chem., Int. Ed.* **2000**, *39*, 592−595.
(18) Shevchenko, E. V.; Talapin, D. V.; Kotov, N. A.; O'Brien, S.; Murray, C. B. Structural diversity in binary nanoparticle superlattices. *Nature* **2006**, *439*, 55−59.
(19) Huang, M. J.; Hsu, C. H.; Wang, J.; Mei, S.; Dong, X. H.; Li, Y. W.; Li, M. X.; Liu, H.; Zhang, W.; Aida, T.; Zhang, W.-B.; Yue, K.; Cheng, S. Z. D. Selective assemblies of giant tetrahedra via precisely controlled positional interactions. *Science* **2015**, *348*, 424−428.
(20) Yue, K.; Huang, M.; Marson, R. L.; He, J.; Huang, J.; Zhou, Z.; Wang, J.; Liu, C.; Yan, X.; Wu, K.; Guo, Z.; Liu, H.; Zhang, W.; Ni, P.; Wesdemiotis, C.; Zhang, W.-B.; Glotzer, S. C.; Cheng, S. Z. D. Geometry induced sequence of nanoscale Frank-Kasper and quasicrystal mesophases in giant surfactants. *Proc. Natl. Acad. Sci. U. S. A.* **2016**, *113*, 14195−14200.
(21) Grason, G. M. *Frank Kasper Phases of Squishable Spheres and Optimal Cell Models*, can be found under http://www.condmatjournalclub.org/?p=2731, 2016.
(22) Percec, V.; Imam, M. R.; Peterca, M.; Wilson, D. A.; Heiney, P. A. Self-assembly of dendritic crowns into chiral supramolecular spheres. *J. Am. Chem. Soc.* **2009**, *131*, 1294−1304.
(23) Percec, V.; Imam, M. R.; Peterca, M.; Wilson, D. A.; Graf, R.; Spiess, H. W.; Balagurusamy, V. S. K.; Heiney, P. A. Self-assembly of dendronized triphenylenes into helical pyramidal columns and chiral spheres. *J. Am. Chem. Soc.* **2009**, *131*, 7662−7677.
(24) Sahoo, D.; Peterca, M.; Aqad, E.; Partridge, B. E.; Heiney, P. A.; Graf, R.; Spiess, H. W.; Zeng, X. B.; Percec, V. Hierarchical self-organization of perylene bisimides into supramolecular spheres and periodic arrays thereof. *J. Am. Chem. Soc.* **2016**, *138*, 14798−14807.
(25) Percec, V.; Ahn, C. H.; Ungar, G.; Yeardley, D. J. P.; Moller, M.; Sheiko, S. S. Controlling polymer shape through the self-assembly of dendritic side-groups. *Nature* **1998**, *391*, 161−164.
(26) Percec, V.; Cho, W. D.; Moller, M.; Prokhorova, S. A.; Ungar, G.; Yeardley, D. J. P. Design and structural analysis of the first spherical monodendron self-organizable in a cubic lattice. *J. Am. Chem. Soc.* **2000**, *122*, 4249−4250.
(27) Talapin, D. V.; Shevchenko, E. V.; Bodnarchuk, M. I.; Ye, X. C.; Chen, J.; Murray, C. B. Quasicrystalline order in self-assembled binary nanoparticle superlattices. *Nature* **2009**, *461*, 964−967.
(28) Ziherl, P.; Kamien, R. D. Maximizing entropy by minimizing area: Towards a new principle of self-organization. *J. Phys. Chem. B* **2001**, *105*, 10147−10158.
(29) Grason, G. M.; DiDonna, B. A.; Kamien, R. D. Geometric theory of diblock copolymer phases. *Phys. Rev. Lett.* **2003**, *91*, 058304.
(30) Ziherl, P.; Kamien, R. D. Soap froths and crystal structures. *Phys. Rev. Lett.* **2000**, *85*, 3528−3531.
(31) Zhang, W.-B.; Yu, X. F.; Wang, C. L.; Sun, H. J.; Hsieh, I. F.; Li, Y. W.; Dong, X. H.; Yue, K.; Van Horn, R.; Cheng, S. Z. D. Molecular nanoparticles are unique elements for macromolecular science: From "nanoatoms" to giant molecules. *Macromolecules* **2014**, *47*, 1221−1239.
(32) Zhang, W.; Huang, M. J.; Su, H.; Zhang, S. Y.; Yue, K.; Dong, X. H.; Li, X. P.; Liu, H.; Zhang, S.; Wesdemiotis, C.; Lotz, B.; Zhang, W.-B.; Cheng, S. Z. D.; Li, Y. Toward controlled hierarchical heterogeneities in giant molecules with precisely arranged nano building blocks. *ACS Cent. Sci.* **2016**, *2*, 48−54.
(33) Yu, X. F.; Yue, K.; Hsieh, I. F.; Li, Y. W.; Dong, X. H.; Liu, C.; Xin, Y.; Wang, H. F.; Shi, A. C.; Newkome, G. R.; Ho, R. M.; Chen, E. Q.; Zhang, W.-B.; Cheng, S. Z. D. Giant surfactants provide a versatile platform for sub-10-nm nanostructure engineering. *Proc. Natl. Acad. Sci. U. S. A.* **2013**, *110*, 10078−10083.
(34) Li, Y. W.; Zhang, W.-B.; Hsieh, I. F.; Zhang, G. L.; Cao, Y.; Li, X. P.; Wesdemiotis, C.; Lotz, B.; Xiong, H. M.; Cheng, S. Z. D. Breaking symmetry toward nonspherical Janus particles based on Polyhedral Oligomeric Silsesquioxanes: molecular design, "click" synthesis, and hierarchical structure. *J. Am. Chem. Soc.* **2011**, *133*, 10712−10715.
(35) Ungar, G.; Percec, V.; Holerca, M. N.; Johansson, G.; Heck, J. A. Heat-shrinking spherical and columnar supramolecular dendrimers: Their interconversion and dependence of their shape on molecular taper angle. *Chem. - Eur. J.* **2000**, *6*, 1258−1266.

DOI: 10.1021/acscentsci.7b00188
ACS Cent. Sci. 2017, 3, 860−867

(36) Percec, V.; Cho, W. D.; Ungar, G. Increasing the diameter of cylindrical and spherical supramolecular dendrimers by decreasing the solid angle of their monodendrons via periphery functionalization. *J. Am. Chem. Soc.* **2000**, *122*, 10273−10281.
(37) Jeener, J.; Meier, B. H.; Bachmann, P.; Ernst, R. R. Investigation of exchange processes by 2-Dimensional nmr-spectroscopy. *J. Chem. Phys.* **1979**, *71*, 4546−4553.
(38) Tomalia, D. A.; Khanna, S. N. A systematic framework and nanoperiodic concept for unifying nanoscience: Hard/soft nanoelements, superatoms, meta-atoms, new emerging properties, periodic property patterns, and predictive Mendeleev-like nanoperiodic tables. *Chem. Rev.* **2016**, *116*, 2705−2774.

DOI: 10.1021/acscentsci.7b00188
ACS Cent. Sci. 2017, 3, 860−867